P 30014

NASA TECHNICAL NOTE **NASA TN D-7501**

NASA TN D-7501

ANALYSIS OF STRESSES AT THE BORE OF A DRILLED BALL OPERATING IN A HIGH-SPEED BEARING

by Harold H. Coe and John E. Lynch

Lewis Research Center

Cleveland, Ohio 44135

NATIONAL AERONAUTICS AND SPACE ADMINISTRATION • WASHINGTON, D. C. • DECEMBER 1973

1. Report No.	2. Government Accession No.	3. Recipient's Catalog No.
NASA TN D-7501		

4. Title and Subtitle	5. Report Date
ANALYSIS OF STRESSES AT THE BORE OF A DRILLED BALL OPERATING IN A HIGH-SPEED BEARING	December 1973
	6. Performing Organization Code
7. Author(s)	8. Performing Organization Report No.
by Harold H. Coe and John E. Lynch	E-7405
	10. Work Unit No.
9. Performing Organization Name and Address	501-24
Lewis Research Center National Aeronautics and Space Administration Cleveland, Ohio 44135	11. Contract or Grant No.
	13. Type of Report and Period Covered
12. Sponsoring Agency Name and Address	Technical Note
National Aeronautics and Space Administration Washington, D. C. 20546	14. Sponsoring Agency Code

15. Supplementary Notes

16. Abstract

Three-dimensional stress distributions were calculated for both a regular drilled ball (50 percent of weight removed) and a drilled ball with a stiffening web. The balls were 20.6 mm (0.8125 in.) in diameter and had a 12.6-mm- (0.496-in.-) diameter concentric hole. The stiffening web was 1.5 mm (0.06 in.) thick. The calculations showed that a large reversing tangential stress at the hole bore was reduced by one-half by the addition of the web.

17. Key Words (Suggested by Author(s))	18. Distribution Statement
Bearings; Ball bearings; Drilled ball; Stress analysis; High speed; Webbed ball	Unclassified - unlimited

19. Security Classif. (of this report)	20. Security Classif. (of this page)	21. No. of Pages	22. Price*
Unclassified	Unclassified	22	Domestic, $2.75 Foreign, $5.25

* For sale by the National Technical Information Service, Springfield, Virginia 22151

ANALYSIS OF STRESSES AT THE BORE OF A DRILLED BALL OPERATING IN A HIGH-SPEED BEARING

by Harold H. Coe and John E. Lynch

Lewis Research Center

SUMMARY

A computational analysis was performed on two drilled-ball configurations to determine the effect of a change in geometry on the three-dimensional stress distributions in the balls. A finite-element technique was used to calculate the stresses in a regular drilled ball (50 percent weight reduction) and in a drilled ball with a stiffening web (46 percent weight reduction). The drilled ball was 20.6 millimeters (0.8125 in.) in diameter and had a 12.6 millimeter-(0.496-in.-) diameter concentric hole. The stiffening web used was 1.5 millimeters (0.06 in.) thick.

The calculations were made for conditions of a drilled ball operating in a 125-millimeter-diameter-bore bearing at a shaft speed of 24 000 rpm (a DN value of 3 million) and at thrust loads of 11 000 and 22 000 newtons (2500 and 5000 lb). These were the approximate conditions under which an experimental drilled-ball bearing of the same size experienced a ball failure due to flexural fatigue.

The analysis shows that a large reversing stress occurs in the bore of the ball as the ball rotates through one complete revolution. At the 22 000 newton-(5000-lb) load condition, the maximum tangential stress at the bore ranges from 470×10^6 newtons per square meter (70 000 psi) in tension to about 150×10^6 newtons per square meter (20 000 psi) in compression.

The addition of the stiffening web reduces the change in tangential stress to about one-half that in the regular drilled ball or 300×10^6 newtons per square meter (45 000 psi) at the 22 000-newton-(5000-lb-) thrust load condition.

INTRODUCTION

Recent trends in gas turbine design have resulted in a requirement for higher shaft speeds and larger shaft diameters (ref. 1). While bearings in current aircraft turbine

engines operate in the range 1.5 to 2.0 million DN (bearing bore in mm multiplied by shaft speed in rpm), bearings in future engines may operate at DN values of 3.0 million or higher. When ball bearings are operated at high DN values, however, centrifugal forces on the outer race produced by the balls can become significant. The resulting increase in Hertz stress at the outer-race contacts can seriously shorten bearing fatigue life (ref. 2).

A possible solution to this high-speed problem is to reduce the mass of the ball and thereby reduce the centrifugal forces (ref. 3). Therefore, bearings with spherically hollow or cylindrically hollow (drilled) balls have been tested (refs. 4 to 8). In these tests, the 17.5-millimeter-(0.6875-in.-) diameter spherically hollow balls with a 1.5-millimeter (0.060-in.) wall thickness (refs. 4 and 5) failed by flexural fatigue in the area of the electron-beam weld. The drilled-ball bearings performed satisfactorily at DN values up to 3 million, as described in references 6 and 7. After accumulating some running time, however, the bearings experienced ball failures, as reported in reference 8. It was concluded that these ball failures were caused by cracks that, because of flexural fatigue, initiated in the bore. To understand these drilled-ball fatigue failures better and to evaluate a proposed ball design change, three-dimensional stress distributions were required.

Therefore, this report describes the computation and analysis of the stresses for a drilled ball and for a drilled ball with a stiffening web. A finite-element technique was utilized for the computation. While the stresses were computed for the complete ball, the analysis is mainly concerned with the stresses at the bore.

The analysis was made for a 20.6-millimeter- (0.8125-in.-) diameter drilled ball under the conditions of operation in a 125-millimeter-diameter-bore ball bearing with an inner-race speed of 24 000 rpm and bearing thrust loads of 11 000 and 22 000 newtons (2500 and 5000 lb). The drilled ball had a 12.6-millimeter- (0.496-in.-) diameter hole (50-percent weight reduction). The drilled ball with a stiffening web had two 12.6-millimeter- (0.496-in.-) diameter holes and a central web, 1.5-millimeters (0.06 in.) thick, between the holes in the center of the ball. The weight reduction for this ball was 46 percent.

ANALYTICAL PROCEDURE

It was decided to calculate the stresses that exist in a ball operating under the conditions noted in reference 8 prior to failure. The 125-millimeter-bore bearing used in reference 8 and considered in this report is shown in figure 1. The specifications for this bearing are shown in table I. The bearing operating conditions as well as the calculated values for ball loads, contact angles, and speeds are shown in table II.

Also considered for analysis was a drilled ball with a stiffening web. The conditions calculated for a bearing with the webbed ball are also shown in table II. Cross sections of the drilled ball and of the ball with a stiffening web are shown in figure 2. The web thickness used was 1.5 millimeters (0.06 in.).

Because of the centrifugal force generated by the balls orbiting about the bearing axis, the inner- and outer-race contact loads and angles become dissimilar, as shown in figure 3. It was for this load configuration that the stresses in the balls were determined.

The spherical balls contain a cylindrical hole. A cylindrical coordinate system is used to locate points within the ball, with the z-axis collinear with the hole centerline (fig. 3).

In this coordinate system, a positive radius vector is directed away from the z-axis and is normal to it. Although the ball geometry is axisymmetric about the z-axis, the loads, deflections, and stresses are dependent on the angle θ, which is measured as shown in figure 3.

STRESS ANALYSIS

A finite-element technique was utilized to calculate the stresses in the ball. The ball was divided into axisymmetric finite ring elements as shown in cross section in figures 4 and 5.

The stress calculations were performed on a digital computer using a ring finite-element program. This program analyzes axisymmetric solids of revolution with arbitrary shape which are subjected to unsymmetrical loadings. It determines elastic deformations, stresses, and strains in a three-dimensional solid which is modeled as an assemblage of rings of regular cross section.

All loads are approximated by Fourier series load terms in the tangential coordinate θ. The three-dimensional equations of elasticity are uncoupled into sets of two-dimensional equations, one set of equations for each Fourier series loading.

Each set of equations is solved for the Fourier nodal deflections and element stress components for that Fourier loading. These Fourier stress components are finally combined to give the r, z, and θ directional stresses for each element at any selected tangential angle.

The number of Fourier terms is arbitrary, but is restricted to 25 for this investigation. A greater number of terms would improve the angular representation of contact loads and contact stresses, at the expense of increased computer time, with little improvement in representing bore stresses according to Saint Venant's principle. Twenty-five Fourier terms appears to be a practical compromise.

Contact Force Representation

The load at a ball contact "point" is actually distributed over an area which depends upon the load magnitude. If treated as a pressure, the load is a function of r, z, and θ within the contact area. However, in the present analysis, the load is represented as a discrete function of r and z and as a continuous function of θ in the following manner. The load is first distributed over a small number of nodal points located in the r, z-plane; these nodes are adjacent to the contact "point." The r or z load component at each nodal point $F_{i,p}(\theta)$ is then approximated as a delta function of angle

$$F_{i,p}(\theta) = F_i \delta(\theta - p) \simeq \lim_{c \to \infty} F_i \frac{\sin c(\theta - p)}{\pi(\theta - p)} \tag{1}$$

where i = r for the radial force component at the node, i = z for the axial force component at the node, $p = 0^o$ for outer-race loads, and $p = 180^o$ for inner-race loads. This angular variation is shown in figure 6.

A finite value of c was selected to define the angular "width" of the contact area, which was then reasonably close to a normal contact dimension. Since the numerical method used for the stress analysis utilizes a Fourier coefficient approach, the Fourier load coefficients must also be obtained. The load component at each nodal point is represented in a Fourier cosine series as

$$F_{i,p}(\theta) = \sum_{n=1}^{n=24} a_n \cos n\theta + \frac{a_o}{2} \tag{2}$$

where the n^{th} Fourier load coefficient is

$$a_n = \frac{1}{\pi} \int_{-\pi}^{+\pi} F_{i,p}(\theta) \cos n\theta \, d\theta \tag{3}$$

Combining equations (1) and (3) gives

$$a_n = \frac{F_i}{\pi} \int_{-\pi}^{+\pi} \frac{\sin c(\theta - p)}{\pi(\theta - p)} \cos n\theta \, d\theta \tag{4}$$

Since the integrand I is an even function of θ, where $I(\theta) = I(-\theta)$,

$$a_n = \frac{2F_i}{\pi^2} \int_0^{\pi} \frac{\sin c\ (\theta - p)}{\theta - p} \cos n\theta\ d\theta \tag{5}$$

These integrals are evaluated for both force components, F_r and F_z, at each node for all 25 values of n. Since

$$\int_{-\pi}^{+\pi} F_{i,p}(\theta)d\theta = \int_{-\pi}^{+\pi} F_i \delta(\theta - p)\ d\theta = F_i \tag{6}$$

the value of F_i in each case is the magnitude of the r or z force component assigned to that node.

Centrifugal Body Force Representation

There are two types of centrifugal body forces (inertia loads) on each element of volume in the ball. The first type of loading results from the rotation of the ball about its own spin axis at speed ω. This rotational axis is the z-axis shown in figure 3. The second type of centrifugal load is produced by the orbital motion of the ball about the shaft centerline at speed Ω. For purposes of computation, the ball spin axis was considered to be always parallel to the shaft axis.

Spin loads. - Each ring element is centered about the ball z-axis and is subjected to radial centrifugal forces which depend on the material density ρ, cross-sectional area A, element radial position r from the z-axis, and the speed of rotation ω about the z-axis. For each ring element, the radially directed force per unit of circumference is

$$F_{spin} = ma = \rho \frac{A}{g} r\ \omega^2 \tag{7}$$

which is directed as shown in figure 7.

Orbital loads. - The orbital load per unit of circumference at angle θ, for a ring element located at ball radius r, and at distance $R(\theta)$ from the shaft centerline, is of magnitude

$$F_{orbital} = ma = \rho \frac{A}{g} R(\theta)\Omega^2 \tag{8}$$

and is directed as shown in figure 7. Note that $F_{orbital}$ is dependent on θ, since $R(\theta)$ for any given r value can be described by

$$R(\theta) = \sqrt{(\bar{R} + r \cos \theta)^2 + (r \sin \theta)^2} \tag{9}$$

where $\bar{R}$ is the bearing pitch radius (fig. 7). If r is small compared to $\bar{R}$, $R(\theta)$ is approximately equal to the pitch radius.

The direction for $F_{orbital}$ is also dependent on θ, but this load can be resolved into two components, along the r and θ directions, as shown in figure 8.

The magnitudes of the two components can be approximated by

$$F_r \cong F_{orbital} \cos \theta \tag{10}$$

$$F_\theta \cong F_{orbital} \sin \theta \tag{11}$$

This approximation assumes that the angle ϕ (fig. 7) is small compared to θ. This approximation is valid when $\bar{R}$ is much greater than r.

The importance of equations (10) and (11) is related to the Fourier representation of forces, which is used in this investigation. Note that if all coefficients except the first are zero in

$$F_r(\theta) = \sum_{n=1}^{24} b_n \cos n\theta + \frac{b_o}{2} \tag{12}$$

and

$$F_\theta(\theta) = \sum_{n=1}^{24} d_n \cos n\theta + \frac{d_o}{2} \tag{13}$$

then

$$F_r(\theta) = b_1 \cos \theta \tag{14}$$

and

$$F_\theta(\theta) = d_1 \sin \theta \tag{15}$$

Equations (14) and (15) match equations (10) and (11), respectively, if b_1 and d_1 are set equal to $F_{orbital}$ as given by equation (8).

This method of approximating the orbital body loads is important since only Fourier coefficients are utilized by the computer program to represent loads. All orbital motion body loads are zero except for those in the set of elasticity equations for which n=1, whereas contact loads are nonzero for all values of n.

In the actual calculations, the stresses due to the spin loads (since they do not depend on the angle θ) were calculated separately from those stresses due to the contact and orbital loads. The total stress then, by superposition, is equal to the sum of the two stress values for any given element.

RESULTS AND DISCUSSION

Stresses in the ball were computed for four cases, as stated previously, for a ball operating in a 125-millimeter-bore bearing. Two cases were for the regular drilled ball as tested in reference 8, and two cases were for a drilled ball with a 1.5-millimeter-(0.06-in.-) thick stiffening web. The actual force components applied to the balls in the analysis are given in table III. The material properties for AISI M-50 steel utilized for the stress calculations are given in table IV. Note that with a ball radius of 10.3 millimeters (0.406 in.) and a bearing pitch radius of 78.7 millimeters (3.1 in.) the maximum angle ϕ (see fig. 7) is 7.5° (when $\theta = 90^{\circ}$). Therefore, the approximate equations (10) and (11), based on the assumption that the angle ϕ is small compared to the angle θ, should be valid.

The regular drilled-ball cases were computed first to determine if the values of calculated stresses were reasonable. Then the drilled-ball-with-web-cases were calculated to determine the effect on stress magnitude of the addition of a stiffening member at the center of the hole. The computer program output included the orthogonal stresses for each finite element at several values of the angle θ (measured from the outer-race contact load position). These stresses are radial stress (r direction), transverse stress (z direction), and tangential stress (θ direction). All calculations were made in U.S. customary units and converted to SI units for the report.

Drilled Ball

The drilled-ball failures noted in reference 8 were attributed to flexural fatigue cracks that initiated in the bore of the ball. Therefore, the calculated stresses along the bore (at $\theta = 0^{\circ}$) are plotted as shown in figure 9, for both the 11 000 and 22 000-newtons

(2500- and 5000-lb) load conditions.

The maximum bore stress is in the tangential (θ) direction and occurs in element 115 (see fig. 4) for the 11 000-newton (2500-lb) load condition. This element is located about 1 millimeter (0.04 in.) from the centerline of the ball on the applied load side. For the 22 000 newton (5000-lb) load condition, the maximum bore stress occurred in element 147, which is about 3 millimeters (0.1 in.) from the ball centerline.

The values of tangential and transverse stress for these two elements with maximum bore stress are plotted as a function of the angle θ in figure 10. Note the large reversing tangential stress that occurs for these elements as the ball rotates through one-half revolution. There are two stress reversals then for each complete ball revolution, one being larger than the other because of the difference in ball contact loads at the inner and outer race.

Experimental work with hollow rollers in reference 9 resulted in a recommendation of about 500×10^6 newtons per square meter (70 000 psi) as the maximum permissible tangential stress level for bearings with rollers subjected to bending fatigue. Reference 10 notes an endurance limit of 620×10^6 newtons per square meter (90 000 psi) for a smooth AISI M-50 specimen. The maximum calculated tangential bore stress for the 22 000-newton (5000-lb) case is about 470×10^6 newtons per square meter (70 000 psi) in tension, and the maximum value for the 11 000-newton (2500-lb) case is about 350×10^6 newtons per square meter (50 000 psi). Note that, while the bearing load is doubled, the stress levels in the ball change by a factor of less than 1.5.

In bending fatigue, the change in stress (stress range) and the maximum effective stress are important in establishing an endurance limit for the material. For the 22 000-newton (5000-lb) case, the largest total change in tangential bore stress is about 620×10^6 newtons per square meter (90 000 psi) and the maximum von Mises - Hencky effective stress at the bore is approximately 410×10^6 newtons per square meter (60 000 psi).

Since the bearings in reference 8 did operate for some time before failure, these calculated values for the stresses in the ball were judged to be reasonable. This judgment in turn added confidence to the method utilized for the stress calculation. Therefore, for comparison, the stresses for the ball with web were also calculated.

Ball With Web

The ball-with-web geometry was chosen as a design to reduce flexure in the drilled ball by adding a stiffening web at the center of the ball. Stress calculations were made to determine the effectiveness of this design change.

The calculated tangential stress along the hole bore (and across the web) is plotted in

figure 11 for both the 11 000- and 22 000-newton (2500- and 5000-lb) conditions. The presence of the web not only reduced the stress level at the bore from that of the regular drilled ball, but also changed the character of the curves as well. The stress values shown are for $\theta = 0^{\circ}$. The maximum bore stress occurred in element 54 (fig. 5) for both load conditions.

Since the changes in stress per revolution of the ball are important for flexural fatigue, values of tangential stress for element 54 were plotted as a function of the angle θ in figure 12. The stresses are shown for both the 11 000- and 22 000-newton (2500- and 5000-lb) conditions.

The maximum calculated value of the tangential stress at the bore for the webbed ball is about 300×10^6 newtons per square meter (45 000 psi) in tension for the 22 000-newton (5000-lb) case and about 240×10^6 newtons per square meter (35 000 psi) for the 11 000-newton (2500-lb) case. The total change in stress with angular position at the 22 000-newton (5000-lb) load is about 300×10^6 newtons per square meter (45 000 psi) for element 54. Note that this stress change for the webbed ball is only about one-half that calculated for the regular drilled ball (fig. 10). Also, note that the maximum tangential stress is only a little more than one-half that of the regular drilled ball. The maximum von Mises - Hencky effective stress at the bore (at $\theta = 0^{\circ}$) was about 250×10^6 newtons per square meter (37 000 psi). Thus, the presence of the web significantly diminishes the large reversing stress that occurs for the drilled ball.

For better visualization, a plot of the tangential stress at the bore, for both the drilled ball and the webbed ball, is presented on polar coordinates in figure 13 for the 11 000-newton (2500-lb) condition. The stress values are for element 115 for the drilled ball (fig. 10) and element 54 for the webbed ball (fig. 12). Note that a tensile stress is plotted radially inward. Since strain is proportional to the stress, this plot gives a representation of the deformation of the ball at the bore surface due to the inner- and outer-race contact loads.

SUMMARY OF RESULTS

A finite-element technique was used to calculate the stresses in a drilled ball and in a ball with a stiffening web. The ball with web was analyzed to determine the effect of a geometry change on the stress. The analysis was made for a 20.6-millimeter-(0.8125-in.-) diameter drilled ball, with a 12.6 millimeter-(0.496-in.-) diameter hole (50-percent weight reduction). The web used was 1.5 millimeters (0.06 in.) thick, which resulted in a ball with a 46-percent weight reduction. The calculations were made for the conditions of a ball operating in a 125-millimeter-bore ball bearing, with a shaft speed of 24 000 rpm and bearing thrust loads of 11 000 and 22 000 newtons (2500 and 5000 lb).

The following results were obtained:

1. The maximum stress calculated for an element at the hole bore was in the tangential direction and occurred at the outer-race contact load position. At the 22 000-newton (5000 lb) bearing load condition, this maximum bore stress ranged from 470×10^6 newtons per square meter (70 000 psi) in tension to 150×10^6 newtons per square meter (20 000 psi) in compression for one revolution of the drilled ball.

2. The introduction of a stiffening web significantly reduces the reversing tangential stress at the hole bore. The total stress change per revolution for the webbed ball was about one-half that for the regular drilled ball.

3. The analysis, made for a bearing ball with nonaxisymmetric loading, resulted in reasonable bore stress values.

Lewis Research Center,
National Aeronautics and Space Administration,
Cleveland, Ohio, August 15, 1973,
501-24.

REFERENCES

1. Brown, P. F.: Discussion of Paper previously published in ASLE Trans. ASLE Trans., vol. 12, no. 3, July 1969, pp. 204-205.

2. Jones, A. B.: The Life of High-Speed Ball Bearings. Trans. ASME, vol. 74, no. 5, July 1952, pp. 695-703.

3. Harris, T. A.: On the Effectiveness of Hollow Balls in High-Speed Thrust Bearings. ASLE Trans., vol. 11, no. 4, Oct. 1968, pp. 290-294.

4. Coe, Harold H.; Parker, Richard J.; and Scibbe, Herbert W.: Evaluation of Electron-Beam-Welded Hollow Balls for High-Speed Ball Bearings. J. Lub. Tech., vol. 93, no. 1, Jan. 1971, pp. 47-59.

5. Coe, Harold H.; Scibbe, Herbert W.; and Parker, Richard J.: Performance of 75-Millimeter-Bore Bearings to 1.8 Million DN with Electron-Beam-Welded Hollow Balls. NASA TN D-5800, 1970.

6. Coe, Harold H.; Scibbe, Herbert W.; and Anderson, William J.: Evaluation of Cylindrically Hollow (Drilled) Balls in Ball Bearings at DN Values to 2.1 Million, NASA TN D-7007, 1971.

7. Holmes, P. W.: Evaluation of Drilled-Ball Bearings at DN Values to Three Million. I - Variable Oil Flow Tests. NASA CR-2004, 1972.

8. Holmes, P. W.: Evaluation of Drilled-Ball Bearings at DM Values to Three Million. II - Experimental Skid Study and Endurance Tests. NASA CR-2005, 1972.

9. Pikovskii, V. A.; Kustov, V. G.; Leonov, E. V.; Shaskin, V. V.; and Zinov'ev, I. V.: Study of the Working Capacity of High-Velocity Radial Bearings with Hollow Rollers. Strength of Materials, vol. 3, no. 10, June 1972, pp. 1178-1185.

10. Sachs, G.; Sell, R.; and Weiss, V.: Tension, Compression, and Fatigue Properties of Several SAE 52100 and Tool Steels Used for Ball Bearings. NASA TN D-239, 1960.

TABLE I. - BEARING SPECIFICATIONS

Bearing outside diameter, mm (in.)	190 (7.48)
Bearing inside diameter, mm (in.)	125 (4.92)
Bearing width, mm (in.)	32.5 (1.28)
Outer-race curvature	0.52
Inner-race curvature	0.52
Number of balls	21
Ball diameter, mm (in.)	20.6 (0.8125)
Ball hole diameter, mm (in.)	12.6 (0.496)
Bearing pitch diameter, mm (in.)	157.5 (6.2)
Retainer type	One piece, with stub pins
Retainer material	AISI 4340, silver plated
Race and ball material	AISI CVM-50

TABLE II. - BEARING OPERATING CONDITIONS

[Shaft speed, 24 000 rpm; ball orbital speed, 10 900 rpm]

Ball geometry	Thrust load		Outer race			Inner race			Ball spin speed rpm
	N	lb	Contact load		Contact angle, deg	Contact load		Contact angle, deg	
			N	lb		N	lb		
Drilled	11 000	2500	2890	670	10.2	1200	270	26.0	95 600
Drilled	22 000	5000	3990	896	15.3	2250	506	28.0	98 400
With web	11 000	2500	3130	704	9.8	1200	270	26.0	95 600
With web	22 000	5000	4140	931	14.8	2250	506	28.0	98 400

TABLE III. - APPLIED FORCE COMPONENTS

Ball geometry	Outer-race contact load				Inner-race contact load			
	r-component		z-component		r-component		z-component	
	N	lb	N	lb	N	lb	N	lb
Drilled	-2930	-659	527	118	-1080	-243	-527	-118
Drilled	-3840	-864	1050	237	-1990	-447	-1050	-237
With web	-3090	-695	527	118	-1080	-243	-527	-118
With web	-4000	-900	1050	237	-1990	-447	-1050	-237

TABLE IV. - MATERIAL PROPERTIES OF AISI M-50 STEEL USED IN CALCULATIONS

Density, kg/m^3 ($lb/in.^3$)	8.0×10^3 (0.29)
Young's modulus, N/m^2 (psi)	2.0×10^{11} (29×10^6)
Poisson's ratio	0.25

Figure 1. - Drilled-ball bearing with 125-millimeter-diameter bore tested in reference 8 and used for analysis in present report.

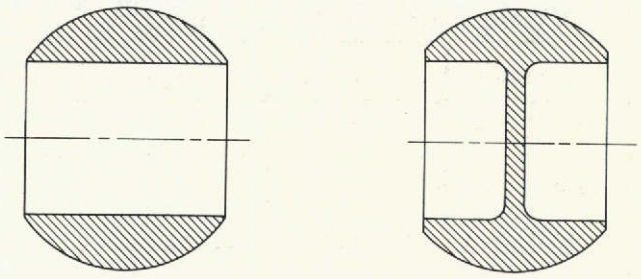

(a) Drilled ball. (b) Ball with web.

Figure 2. - Cross section of ball configurations used for stress analysis.

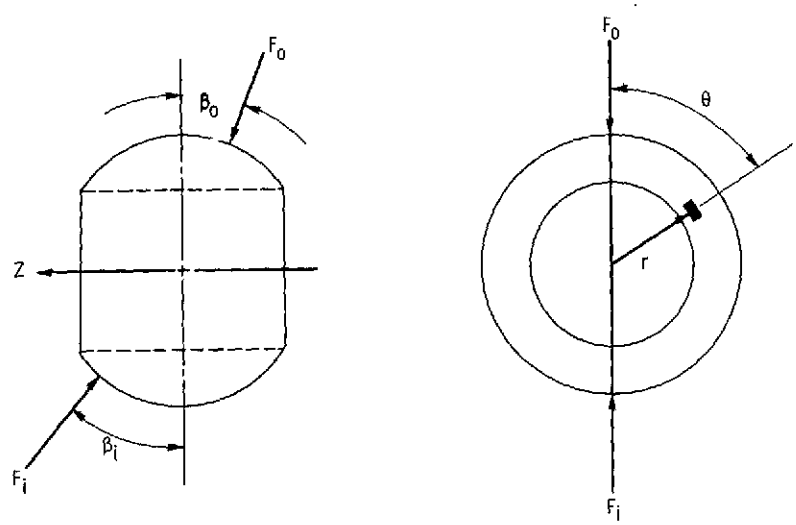

Figure 3. - Ball contact loads and angles at operating conditions and cylindrical coordinate system used for analysis.

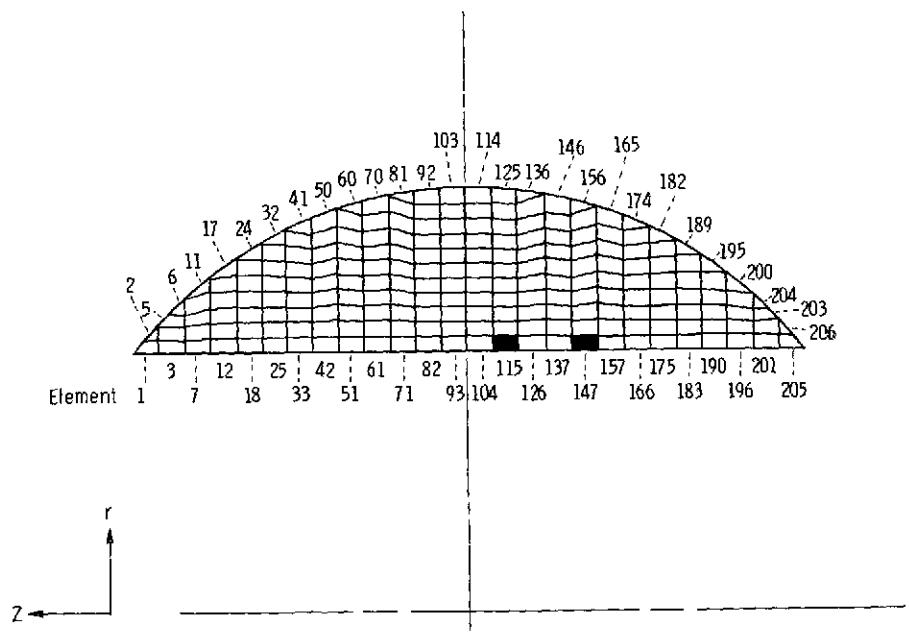

Figure 4. - Finite-element mesh for drilled ball in r, Z-plane.

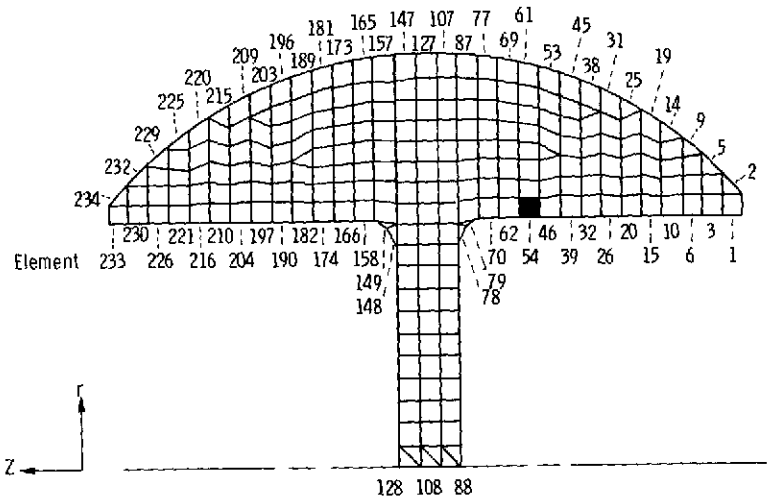

Figure 5. - Finite-element mesh for ball with web in r,Z-plane.

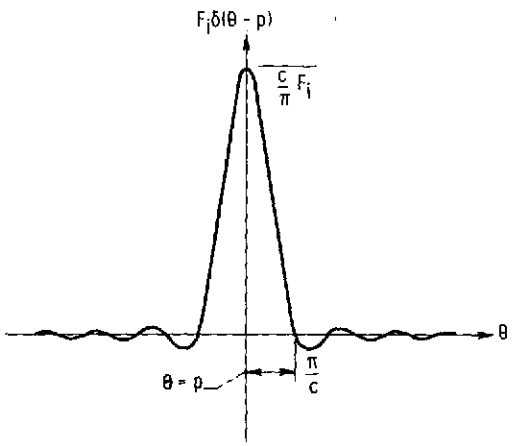

Figure 6. - Contact force distribution as function of angle from outer-race load position θ.

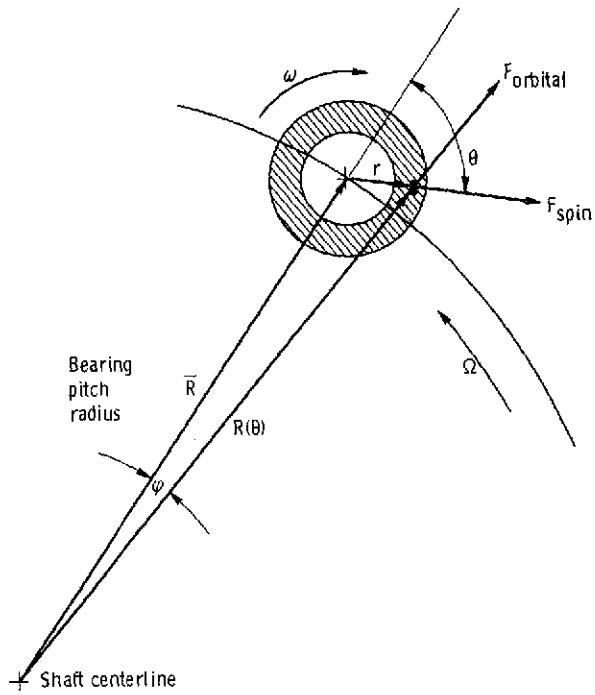

Figure 7. - Directions for spin and orbital loads per unit circumference of ring element at distance R(θ) from shaft centerline.

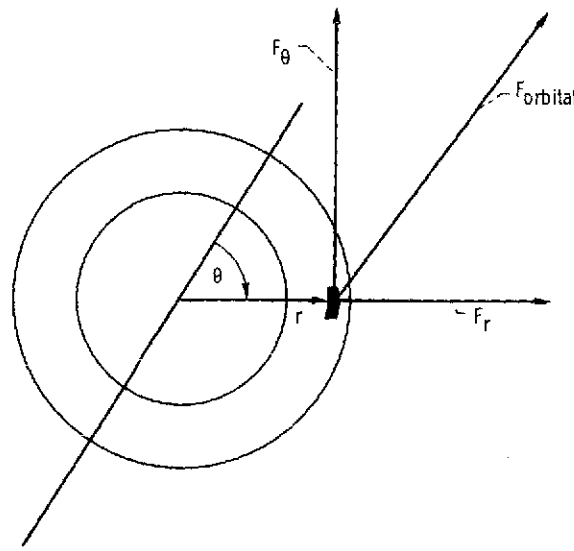

Figure 8. - Components of orbital body load per unit circumference of ring element at position r, θ in ball.

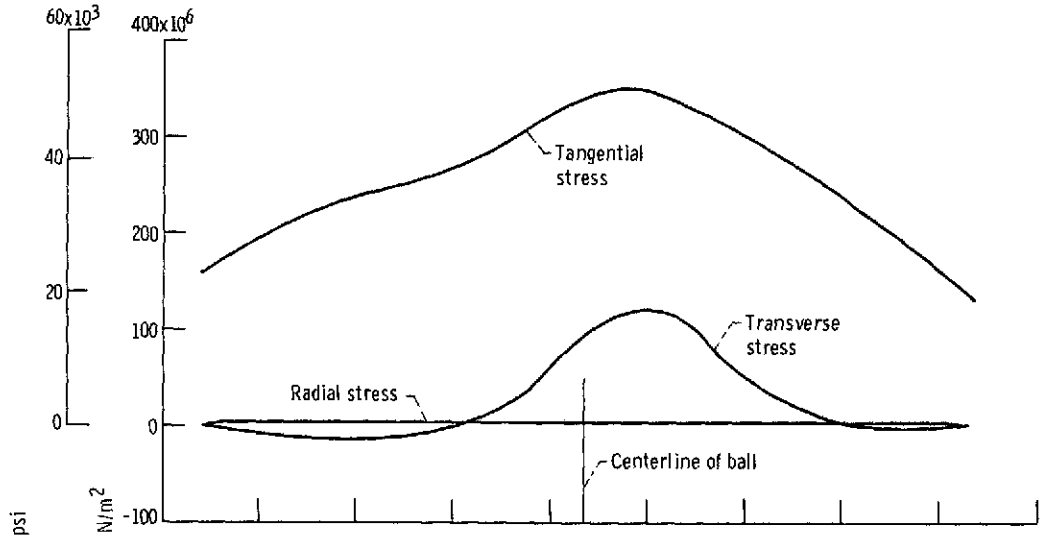

(a) Bearing load, 11 000 newtons (2500 lb).

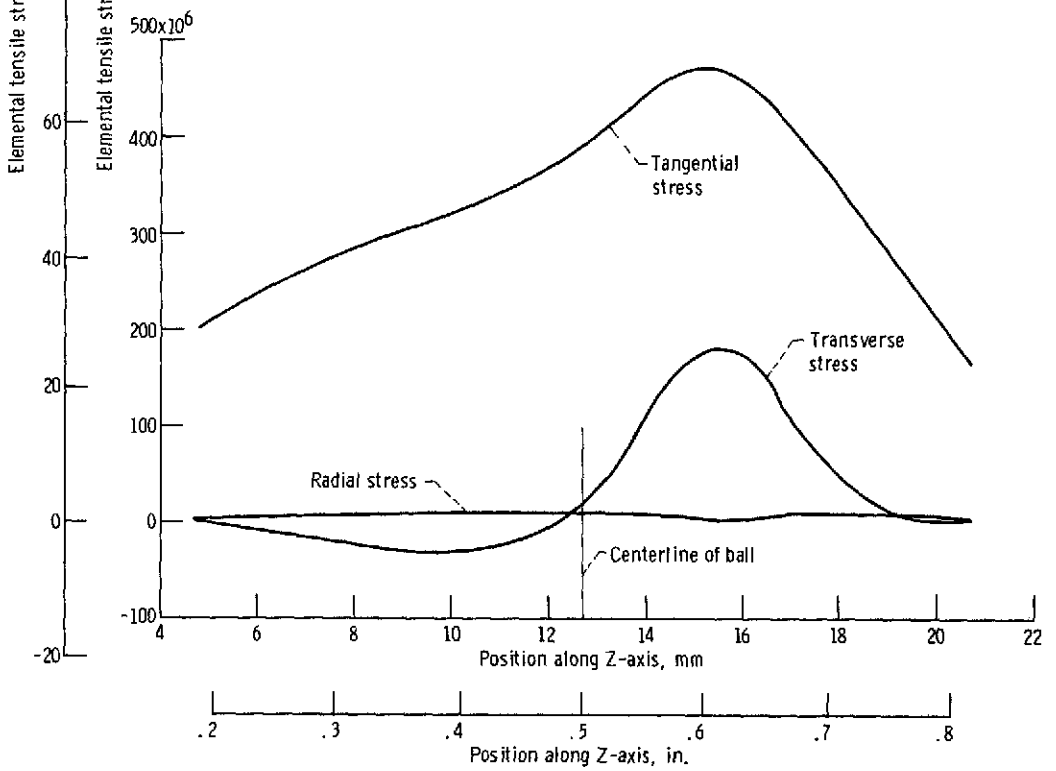

(b) Bearing load, 22 000 newtons (5000 lb).

Figure 9. - Stresses along bore of drilled ball. Angle from outer-race load position $\theta = 0^{0}$.

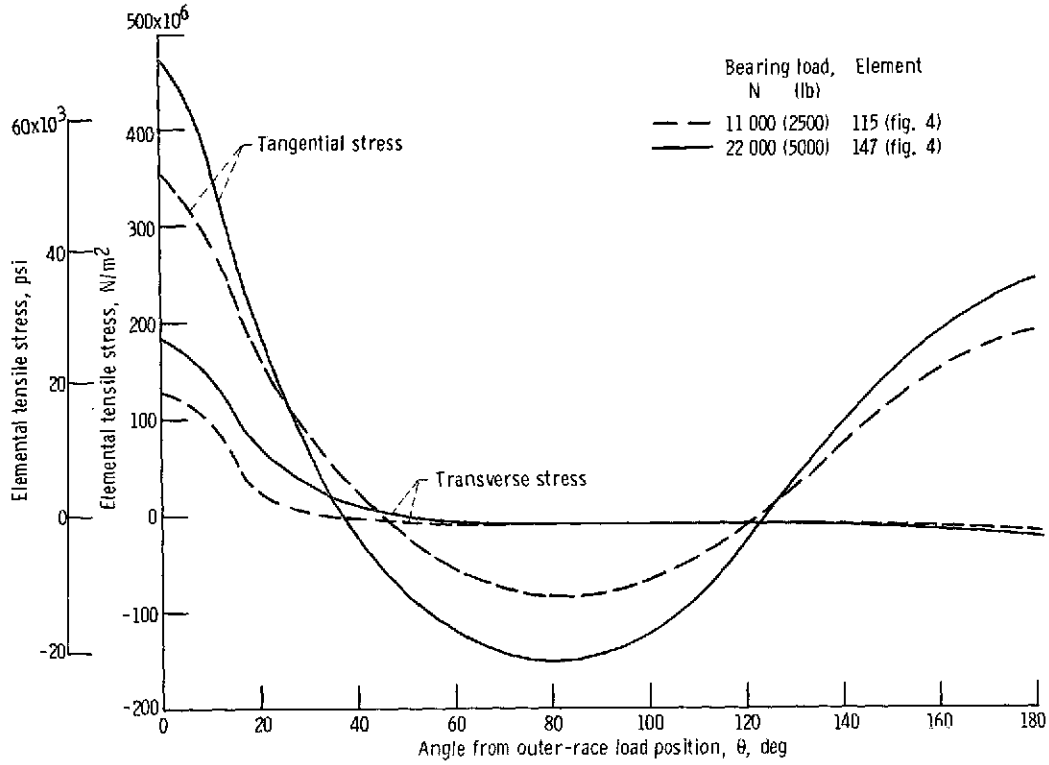

Figure 10. - Stress at bore of drilled ball as function of angle from outer-race load position θ. Elements for maximum stress at θ = 0°.

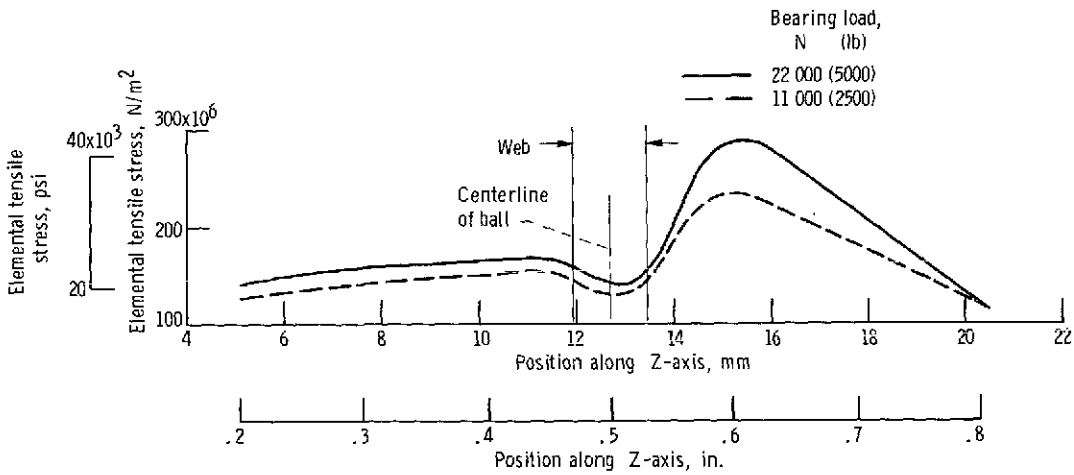

Figure 11. - Tangential stress along bore of ball with web at angle from outer-race load position θ of 0° for two loads.

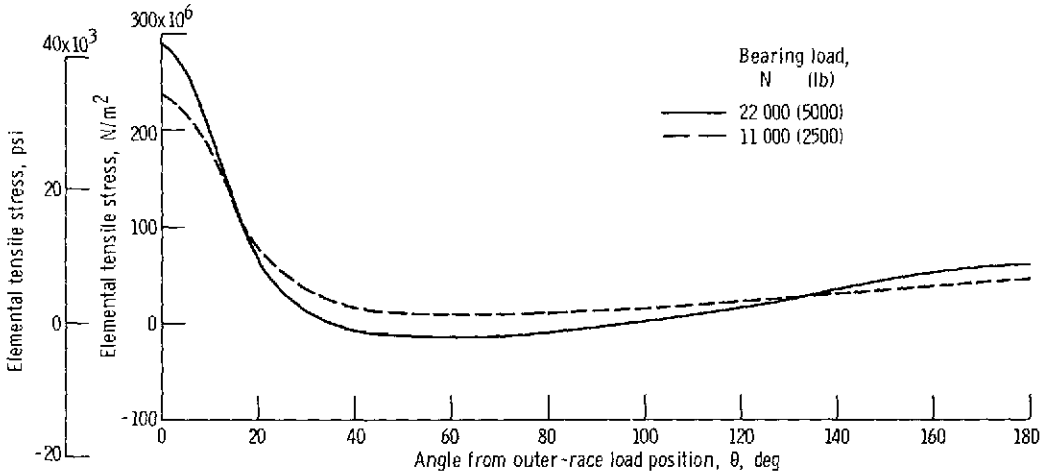

Figure 12. - Tangential stress at bore of ball with web, as function of angle from outer-race load position θ for element with maximum bore stress at $\theta = 0^0$ (element 54, fig. 5).

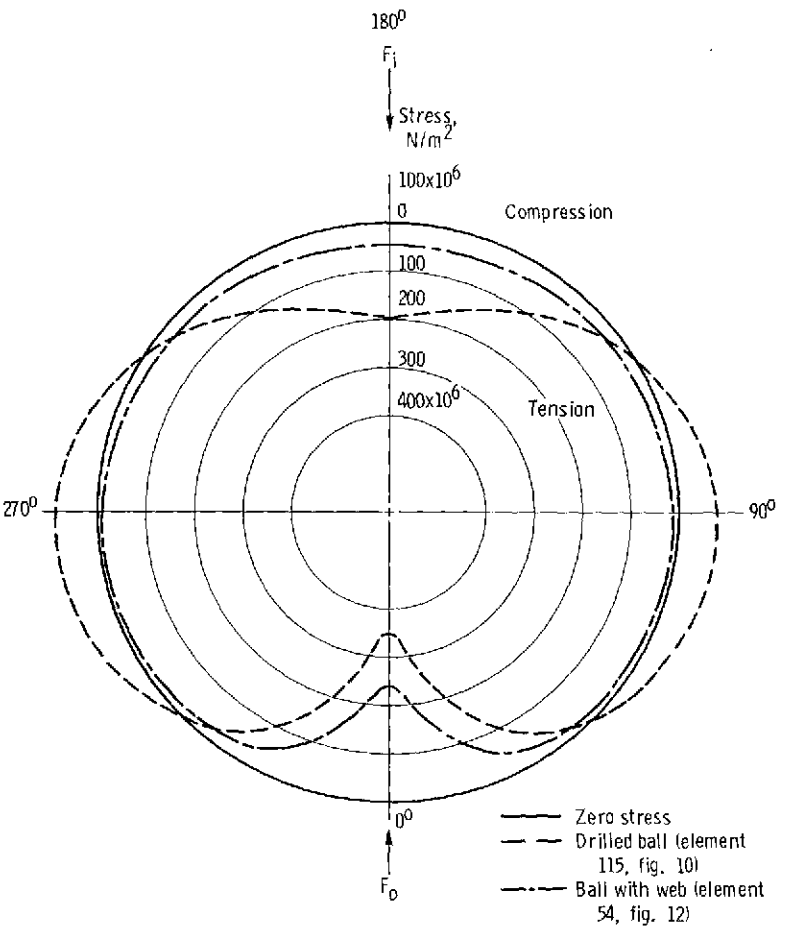

Figure 13. - Tangential stress at bore of bearing ball as function of angle from outer-race load position θ. Bearing load, 11 000 newtons (2500 lb).